Dalton Transactions

An international journal of inorganic chemistry

Accepted Manuscript

This article can be cited before page numbers have been issued, to do this please use: R. Ramasubramanian, K. Anandababu, N. C. Moesch-Zanetti, F. Belaj and M. Ramasamy, *Dalton Trans.*, 2019, DOI: 10.1039/C9DT02518A.

ROYAL SOCIETY OF CHEMISTRY

rsc.li/dalton

View Article Online
DOI: 10.1039/C9DT02518A

Bioinspired Models for an Unusual 3-Histidine Motif of Diketone Dioxygenase Enzymes

Ramamoorthy Ramasubramanian,[a] Karunanithi Anandababu,[a] Nadia C. Mösch-Zanetti,[b] Ferdinand Belaj [b] and Ramasamy Mayilmurugan[a]*

[a]Bioinorganic Chemistry Laboratory/Physical Chemistry, School of Chemistry, Madurai Kamaraj University, Madurai- 625021, India. mayilmurugan.chem@mkuniversity.org
[b]Institute of Chemistry, University of Graz, Schubertstrasse 1, 8010 Graz, Austria.

Abstract: Bioinspired models for contrasting electronic nature of neutral tris-histidine from the anionic 2-histidine-1-carboxylate facial motif and their subsequent impact on catalysis is reported. Herewith, iron(II) complexes $[Fe(L)(CH_3CN)_3](SO_3CF_3)_2$ 1 - 3 of tris(2-pyridyl)-based ligands(L) have been synthesized and characterized as the accurate structural models for the neutral 3-histidine triad of the diketone dioxygenases enzyme (DKDO). The molecular structure of one of the complexes exhibits octahedral coordination geometry and Fe-$N11_{py}$ [1.952(4) - 1.959(4) Å] bond lengths close to Fe-N_{His} (1.98 Å) bond distances of the 3-His-triad in the rest state of enzyme obtained by EXAFS studies. The diketonate substrate-adduct complexes $[Fe(L)(acac^R)](SO_3CF_3)$ (R = Me, Ph) of 1 - 3 have been obtained using $Na(acac^R)$ in acetonitrile. The $Fe^{2+/3+}$ redox potential of complexes (1.05 - 1. 2 V vs. Fc/Fc^+) and their substrate adducts (1.02 - 1.19 V vs. Fc/Fc^+) appeared at almost the same redox barrier. All diketonate adducts exhibit two Fe(II) → acac MLCT bands around 338 - 348 and 430 - 490 nm. Exposure of these adducts to O_2 results in the decay of both MLCT bands with the rate of (k_{O2}) 5.37 - 9.41 × 10^{-3} $M^{-1}s^{-1}$. The k_{O2} values have been concomitantly accelerated 20 - 50 fold by the addition of H^+ (acetic acid), which nicely models the rate enhancement in enzyme kinetics by the glutamate residue (Glu98). The oxygenation of the phenyl substituted adducts yielded benzoin and benzoic acid (40 - 71%) as cleavage products in the presence of H^+ ions. The isotope-labeling experiments using $^{18}O_2$ showed 47% incorporation of ^{18}O in benzoic acid, reveals that oxygen is originated from dioxygen. Thus, the present model complexes exhibit very similar chemical surroundings as in the active site of DKDO and mimic its function elegantly. On the basis of these results, C-C bond cleavage reaction mechanism is discussed.

View Article Online
DOI: 10.1039/C9DT02518A

Introduction

Dioxygenation is one of the important processes in bioremediation for toxic pollutants by heme and non-heme iron enzymes.[1] Especially, a class of non-heme iron enzymes, like catechol dioxygenases are capable of breaking aromatic carbon-carbon bonds by incorporating both atoms of dioxygen.[2] Another major class of O_2-activating enzymes is α-keto acid-dependent dioxygenases which perform oxidative decarboxylation of α-keto acids.[3] While the enzymology and biomimetic chemistry of these enzymes were extensively studied,[2,3] those of the recently discovered non-heme dioxygenases like acireductone dioxygenase (ARD),[4-7] quercetin 2,3-dioxygenase (QD)[8] and β-diketone dioxygenases (DKDO)[9,10] are in a rudimentary stage. They are known to break more challenging aliphatic C-C bonds using O_2. Among these enzymes, DKDO is unique as its active site consists of a redox-active iron(II) center which is coordinated to a 3-histidine facial triad (His-62, His-64, and His-104; Scheme 1) in contrast to the often noted 2-histidine-1-carboxylate facial motif in several other non-heme iron enzymes.[9-17] The remaining coordination sites at iron are speculated as being water molecules.[11-17] The occurrence of the 3-His-triad is surprising because the anionic carboxylate of the 2-histidine-1-carboxylate residue is known to stabilize high valent iron.[3,16] DKDO catalyzes C-C bond cleavage in β-diketones by incorporating O_2 and converting them into nontoxic compounds.[10-18] In fact, the mechanism is not well understood. Particularly, an open question remains whether the cleavage of the C-C bond proceeds *via* Fe(II)-mediated initial substrate activation or *via* O_2 activation.[15-17,19] In addition to biochemical studies of the enzyme, the development of synthetic models is crucial for the elucidation of mechanistic details.

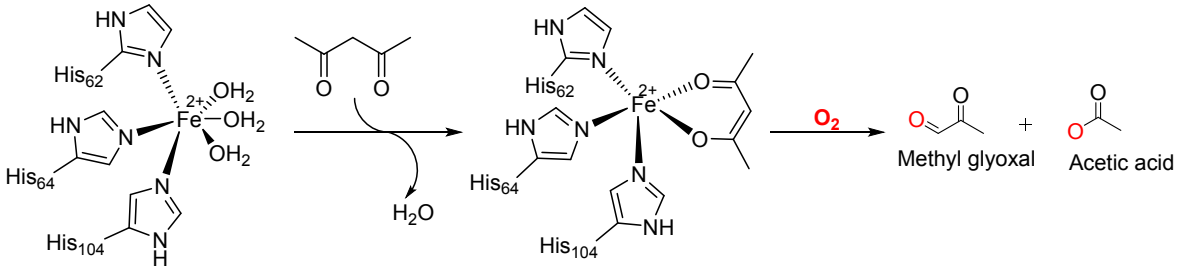

Scheme 1. Active site structure of DKDO and adduct and dioxygenation reaction.

In order to simulate the 3-His-triad hydridotris(3,5-R_2-pyrazol-1-yl)borato ligand (Tp^{R2}) has been successfully applied.[19-22] Kitajima and co-workers have first reported the iron complex [Fe(Tp^{iPr2})(acac)] (acac = acetyl-acetonato) without better bioinorganic outlook.[19] Later,

View Article Online
DOI: 10.1039/C9DT02518A

pioneering efforts of Limberg and co-workers[20] and Fiedler and co-workers,[21,22] iron(II) complexes of $Tp^{Me2/Ph2}$ ligand and its derivatives have been projected as successful models for DKDO. However, they are utilizing boron and phosphorus in the ligand backbone which are proposed for stabilizing high valent iron-oxo species.[2b,19-22] Recently, we have developed the biomimetic models for ARD and Ni(II)-substituted DKDO enzymes using 2,6-bis(1-methyl-benzimidazolyl)pyridine based ligands.[23] In this article, we are reporting novel tris(2-pyridyl) based ligand systems (Scheme 2) that exhibit very similar chemical surroundings as in the active site geometry of DKDO. Our model systems duplicate the coordination environment of the neutral 3-His-triad in DKDO. Furthermore, we demonstrate reactivity towards aliphatic C-C bond cleavage in β-diketones using molecular oxygen. The three pyridine arms of the ligand are expected to mimic the role of the neutral histidine residues in the 3-His motif. In fact, the ligand architecture was reported by us to duplicate structural and functional aspects of cysteine dioxygenase (CDO), whose active site also containing 3-His motif.[23]

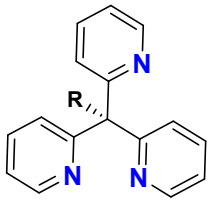

L1, R = Me
L2, R = -OH
L3, R= -OMe

Scheme 2. The structure of ligands used.

Results and Discussion

Synthesis and Characterization: The tris(2-pyridine) based ligands tris(2-pyridyl)ethane (L1), tris(2-pyridyl)methanol (L2) and tris(2-pyridyl)-methoxymethane (L3) were synthesized according to the previous reports with suitable modifications at -78˚C in THF.[24] The model iron(II) complexes were synthesized by the reaction of $Fe(SO_3CF_3)_2$ with the respective ligands in acetonitrile under an argon atmosphere. The complexes $[Fe(L1)(CH_3CN)_3](SO_3CF_3)_2$ 1, $[Fe(L2)(CH_3CN)_3](SO_3CF_3)_2$ 2 and $[Fe(L3)(CH_3CN)_3](SO_3CF_3)_2$ 3 were obtained as red-orange solids in very good yields (74 - 82 %). Recrystallization of complexes 1 - 3 in acetonitrile yielded pure complexes for further studies. The elemental and mass spectrometry analyses confirm their formation. The HR-ESI showed prominent molecular ion peaks for 1: $[C_{18}H_{15}F_3FeN_3O_3S]^+$ *m/z*, 466.01309; 2: $[C_{17}H_{13}F_3FeN_3O_4S]^+$ *m/z*, 467.99263 and 3: $[C_{18}H_{15}F_3FeN_3O_4S]^+$ *m/z*, 482.00788

View Article Online
DOI: 10.1039/C9DT02518A

(Figure S2-S4). The loss of coordinated CH_3CN may be due to dissociation in the spectrometer. The magnetic susceptibility measurements for 1 - 3 by Evan's method showed μ_{eff} = 5.1 - 5.4 μ_B, which is close to the spin-only value of a high-spin iron(II) center (S = 2). In fact, they exhibited paramagnetically shifted broad ^{1}HNMR peaks in CD_3CN. However, the use of non-coordinating solvents CH_2Cl_2 and in $CHCl_3$ for the synthesis of complexes resulted in the formation of bis-complex of type $[Fe(L)_2](CF_3SO_3)_2$. The substrate adducts of 1 - 3 were obtained by reaction of the ligands L1 - L3 with $Fe(SO_3CF_3)_2$ followed by addition of $Na(acac^{R1})$ (R_1 = Me, Ph) in acetonitrile under an argon atmosphere (Scheme 3) and the solution was filtered to remove $NaSO_3CF_3$ and then evacuated to yield red-orange solids. The solids were washed with diethyl ether (3 × 3mL) and dried under *vacuum.* The complexes were redissolved in CH_3CN and recrystallized by layering with diethyl ether yielded pure adducts with moderate yields (49 - 61%). All adducts were isolated as brown-red solids and characterized by ESI-MS or HR-ESI mass as $[Fe(L1)(acac^{Me})](SO_3CF_3)$ 1a: *m/z,* 416.11 for $[Fe(L1)(acac^{Me})]^+$; $[Fe(L1)(acac^{Ph})](SO_3CF_3)$ 1b: *m/z*, 541.9780 for $[Fe(L1)(acac^{Ph})]^+$; $[Fe(L2)(acac^{Me})](SO_3CF_3)$ 2a: *m/z*, 417.70 for $[Fe(L2)(acac^{Me})]^+$; $[Fe(L2)(acac^{Ph})](SO_3CF_3)$ 2b: *m/z*, 541.6120 for $[Fe^{II}(L2)(acac^{Ph})]^+$ and $[Fe(L3)(acac^{Me})](SO_3CF_3)$ 3a: *m/z*, 432.0536 for $[Fe(L3)(acac^{Me})]^+$ (Figure S5-S9). The mass analysis clearly reveals the formation of adducts with five-coordinate geometry and sixth coordination may be vacant or occupied by a solvent molecule. It is further confirmed by elemental analysis. However, isolation of the phenyl substituted adduct of 3 was unsuccessful. All the adducts showed the characteristic carbonyls stretching frequencies around 1600 – 1630 cm^{-1} (Figure S10). These complexes 1a – 3a further shown to be EPR silent even at 10 K.

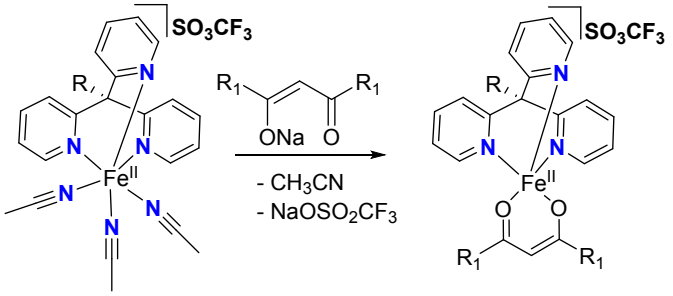

1, R = Me
2, R = -OH
3, R= -OMe

1a, R, R_1 = Me, Me
1b, R, R_1 = Me, Ph
2a, R, R_1 = -OH, Me
2b, R, R_1 = -OH, Ph
3a, R, R_1 = -OMe, Me
3b, R, R_1 = -OMe, Ph

Scheme 3. Synthesis of Fe(II)-complexes and their adducts.

View Article Online
DOI: 10.1039/C9DT02518A

Molecular Structure of 1 and Relevance to DKDO: The suitable single crystal of 1 for X-ray studies were obtained from recrystallization and exhibits an octahedral coordination geometry around the Fe^{II}-center. There are two crystallographically independent complex molecules with the same chemical formulae present in the asymmetric unit cell, both exhibiting the same coordination geometry but slightly different bond lengths and bond angles are observed. The three pyridine nitrogen atoms of L1 and three acetonitrile molecules occupy six coordination sites *via* facial coordination mode. The structure exhibited pseudo-centrosymmetric: If the structure is shifted in the unit cell that the cations are arranged around an inversion center then the cations and two anions (including S1, S2) showed a centrosymmetric sub-structure. The bond angles at N(11)-Fe(1)-N(1), N(21)-Fe(1)-N(2) and N(31)-Fe(1)-N(3) are 179.01(18)˚, 177.98(19)˚ and 178.70(18)˚ respectively and are slightly deviated from 180˚, which reveals a slight distortion from perfect octahedral geometry. The equatorial bonds Fe-$N11_{py}$, 1.959(4) Å and Fe-$N31_{py}$, 1.958(4) Å are slightly longer than the axial bonds Fe-$N21_{py}$, 1.952(4) Å (Table 1). Most interestingly, the Fe-N_{py} bond lengths are almost identical to the Fe-N_{His} bond distances of the DKDO active site (Fe-N_{His} 1.98 Å) determined by EXAFS analysis for the enzyme isolated from *Burkholderia xenovorans* bacteria.[25] In the absence of available X-ray structural parameters for the DKDO enzyme, therefore here presented information is extremely valuable. Furthermore, the Fe-N bond lengths of 1 are shorter than those of the Fe(II)Tp complexes and their derivatives (2.096 - 2.260 Å).[20-22] Thus, 1 represents the first example of a structurally well-defined iron(II) complex with similar coordination geometry and chemical surroundings as in DKDO. The similarity of the Fe^{II} model with that of the enzyme is visualized by the superposition of 1 on the active site structure of DKDO (Figure 1). The main difference between the two geometries is the torsion around the Fe-N axes, enforced by the rigidity of the tripodal structure of the ligand.

Electronic Spectral and Redox Properties: The complexes 1 - 3 and their substrate adducts (1a - 3a) were subjected to UV-Vis spectroscopic analysis (Table 2, Figure S11-S15). 1 - 3 showed Fe(II)-to-ligand charge transfer (MLCT) transitions at 418 - 438 and 345 - 386 nm[14-17] along with the ligand-based transitions around 205 - 341 nm. However, the complex-substrate adducts showed MLCT transitions around 430 - 490 nm and 348 - 317 nm. They possibly originate from d-orbitals of iron(II)-to *p*-orbitals of the β-keto-enolate and trispyridine. Similar to the enzyme-acac adduct, the positive charge on iron(II)-center decreases the energy of the d-orbital manifold and results in the shift to the higher wavelength of its Fe(II)-to-acac (acac-monoanionic) MLCT transitions.[14,15]

View Article Online
DOI: 10.1039/C9DT02518A

Further, the energies of MLCT transitions are significantly affected by substituents on the substrate. The electron-withdrawing phenyl groups in 1b and 2b are expected to decrease the energy gap of d-orbitals of iron(II) and p-orbitals of $acac^{Ph}$. This results in a redshift of MLCT band compared to their respective methyl-substituted adducts. The electronic spectra of these adducts are consistent with native DKDO enzyme with similar iron(II)-to-enolate MLCT transition transitions at 355 and 420 nm for the $acac^{Me}$ substrate.[14] The Fe^{2+}/Fe^{3+} redox potential of complexes was measured by cyclic voltammetry (CV) and differential pulse voltammetry (DPV) in acetonitrile using Pt-disc and Ag/Ag^{+} as working and reference electrodes respectively. The $Fe^{2+/3+}$ (vs. Fc/Fc^{+}) redox potential of 1 (1.05 V) is slightly lower than those of 2 (1.32 V) and 3 (1.20 V) (Table 2, Figure S16-S18). In CV, the $Fe^{2+/3+}$ redox couples appear far away from reversibility. The $Fe^{2+/3+}$ redox potential of the complexes and their respective adducts 1a-3a ($E_{1/2}$, 1.03 - 1.32 V vs. Fc/Fc^{+}) was found to be very similar and have irreversible redox couple (Table 2, Figure S19-S22). These redox potentials are much higher than a reported redox barrier for the O_2-activation by non-heme iron centers (less than -0.10 V).[26] Furthermore, these $Fe^{2+/3+}$ redox potential of adducts are more positive than those of reported for Fe(II)Tp-adducts (-0.34 to -0.58 V).[21,22]

Dioxygenation Reactions and Kinetic Studies: The reactivity of adducts toward dioxygen was investigated by monitoring the decay of the Fe(II) $\rightarrow$ acac MLCT band (λ_{max} 430, 490 nm) in acetonitrile/acetate buffer. The freshly prepared substrate adducts in acetonitrile were used (formation was confirmed by ESI-MS before O_2 treatment). On treating the methyl-substituted adduct (1a - 3a) with excess O_2 in acetonitrile at 25˚C, the intensity of $Fe^{II}\rightarrow acac^{Me}$ MLCT band decreased with pseudo-first-order reaction rate k_{obs} = 3.83 - 7.34 × 10^{-5} s^{-1} (Table S2, Figure S23-S25). This decay of the MLCT transition indicates the progress of the dioxygenation reaction. The k_{O2} (= $k_{obs}/[O_2]$) values were calculated by including dissolved oxygen concentration in acetonitrile, 8.1 × 10^{-3} M.[28] The adduct 1a showed a higher k_{O2} value (9.41 × 10^{-3} $M^{-1}s^{-1}$) than 2a (4.92 × 10^{-3} $M^{-1}s^{-1}$) and 3a (5.37 × 10^{-3} $M^{-1}s^{-1}$) (Table S2, Figure S26-S28) around pH, 7.4. No such decrease in intensity of the MLCT band was noticed for phenyl substituted adducts (1b - 3b). Interestingly, the dioxygenation reaction rates of 1a - 3a have been increased to 20 – 50 fold (k_{O2}, 110.24 - 460 × 10^{-3} $M^{-1}s^{-1}$) by the addition of 0.5 equivalent H^{+} (acetic acid), whereupon the pH of reaction mixtures decreased to around 5.3 - 5.4 (Table S2, Figure 2, S29-S32) in acetonitrile/acetate buffer. Furthermore, the less reactive bulky phenyl substituted adducts 1b -3b

View Article Online
DOI: 10.1039/C9DT02518A

turn to be reactive at this acidic pH, however, the reaction rates (k_{O2}, 0.08 - 3.32 × 10^{-4} M^{-1} s^{-1}) are slower than those of 1a -3a (Table S2, Figure S33-S36). This H^+ assisted enhancement of reaction rates is very interesting because a glutamate (Glu98) residue is believed to enhance the dioxygenation reaction rate in DKDO enzyme kinetics. In DKDO, Glu98 is located in the secondary coordination sphere of the iron center and promoting both substrate binding and O_2 reduction.[13-15] The Glu98 is connected to the nitrogen of His104 *via* H-bond at a distance of 2.86 Å.[15b]

The dioxygenation reaction rates were observed for 1a – 3a many-fold higher than those of Fe(II)Tp-adducts in toluene.[21-22] Nevertheless, these rates are lower than those of the native enzyme (k_{cat}, 8.5 s^{-1}).[10,11] The k_{O2} value for 1a was measured over a wide range of pH (5.4 - 7.4), which is increased by lowering the pH of the acetonitrile/acetate buffer solution (Table S3, Figure 2B, S37 - S41). The reaction rate saturated at pH 5.4 where it showed the highest k_{O2} value of 466 × 10^{-3} M^{-1} s^{-1}. On the other hand, dioxygenation was completely inhibited at pH values higher than 7.0. It is interesting that the plot of pH vs k_{O2} is similar to that obtained for the DKDO enzyme kinetics (Figure 2B).[15a] This result consistent with the impact of acid-base catalysis by secondary coordination residues (hydrophobic and hydrophilic) as in native enzyme which alters the rates of reactions.[15] Furthermore, adducts of Fe^{3+}, Mn^{2+}, $Cu^{2+,}$ and Zn^{2+} using ligand L1 exhibited no dioxygenation reaction kinetics and no cleavage products formation were observed even after seven days (Figure S42-S45). Similar non-reactive behavior of acac substrates was found with a solution of L1 in the absence of metal. Thus, only the redox-active Fe^{2+} center appears to facilitate C-C bond breaking, which is similar to the enzyme kinetics reported by Straganz and Nidetzky.[13-15]

Additional mechanistic information has been obtained by using stronger oxidizing sources such as *tert*-butyl hydroperoxide (*t*-BuOOH) and $PhI(OAc)_2$ as spectroscopic probes. The treatment of adducts 1a - 3a with 10 equivalents of *t*-BuOOH in acetonitrile at 25˚C showed the decrease in intensity of the Fe^{II} → acac MLCT bands with pseudo-first-order reaction rates k_{obs}, 63.25 - 159.29 × 10^{-5} s^{-1} (Table S2, Figure 3, S46-S49). Upon addition of 0.5 equivalent H^+ (acetic acid) the rate increased approximately 3-fold k_{obs} 156.6 – 412.3 × 10^{-5} s^{-1}. Less reactivity has been observed for the adducts 1b - 3b with *t*-BuOOH, but again, they turned to be reactive by adding 0.5 equivalent of H^+ (acetic acid) and showed k_{obs} values of 1.48 - 12.8 × 10^{-5} s^{-1} (Table S2, Figure S50-S55). As expected, the reaction rates for bulkier 1b - 3b are drastically lower as compared to 1a - 3a. However, all k_{obs} values obtained using *t*-BuOOH are relatively higher than those of O_2

View Article Online
DOI: 10.1039/C9DT02518A

kinetics. Whereas, treatment of 1 - 3 with *t*-BuOOH led to an immediate color change to green which can be assigned to a Fe^{3+}-alkylperoxido species with a *t*-$BuOO^- \rightarrow Fe^{3+}$ LMCT transition around 687-690 nm (Figure 3, S56-S59). Its intensity started to decrease with k_{obs} values of 53.72 - 66.67 $\times 10^{-5}$ s^{-1} at 25° C. The ESI-MS analysis of 2 with *t*-BuOOH revealed a mass cluster at *m/z* = 727.09 corresponds to $[Fe(L2)(t\text{-}BuOO^-)(SO_3CF_3)_2]Na^+$ (Figure S60). The EPR spectra of 3 with *t*-BuOOH measured in methanol showed signals for *high-spin* Fe^{III} (S = 5/2) (*g*, 7.42, 4.29), a rhombic *low-spin* Fe^{III} (*S* = ½) (*g*, 2.47, 2.15, 1.92) (Figure S61). The *high-spin* Fe^{III} is possibly formed via rapid decay of low-spin species. Interestingly, while treating complex-substrate adducts (1a-3a) with *t*-BuOOH showed no such LMCT transition and EPR signals, which is indicating that the absence of the Fe^{3+}-O_2^- type species formation. Furthermore, very similar kinetic information has been obtained on treating complex-substrate adducts with $PhI(OAc)_2$ as an oxidizing source (Table S2, Figure S62-S69). The k_{obs} values were obtained in the range of 1.27 - 140.3 $\times 10^{-5}$ s^{-1} but they are lower than those of the O_2 kinetics.

Product Analysis and Dioxygenation Mechanism: In separate experiments, 1b treated with excess O_2 in the presence of acetic acid over 12 hours. The EPR analysis of the dioxygenation reaction of 1b at 77 K found silent during the course of the reaction.[30b] After that the reaction mixture was analyzed by ESI-MS and showed products benzoin (A) and benzoic acid (B) bound iron(II) complexes, bis-iron(II) complex (Figure S70, S71) along with unidentified products. The time-dependent differential pulse voltammetry studies for 3a with dioxygen showed no concomitant changes in redox potential was observed over 1 hour (Figure S72). Therefore, these results invariably suggest that the oxidation state of Fe(II) center does not varied during the course of the dioxygenation reaction. A very similar observation was reported by Limberg and co-workers for the reaction of $[Fe(Tp^{Me/Ph})(acac)]$ with dioxygen.[20] On the contrary, in the absence of O_2 even with an excess of H_2O, no cleavage products were isolated under the identical condition, hence hydrolytic type mechanistic pathway could be eliminated.

Further, the cleavage products were separated as A (42%) and B (29%) (Scheme 3) and characterized by $^1H/^{13}C$ NMR and GC-MS spectra (Figure S73-S77). The adduct 1b yielded a higher amount of cleavage products (71%) than 2b (50%) and 3b (40%). The product yield has been increased (B, 42%; benzil C, 46%) for 1b on using *t*-BuOOH over 3 hours. Further addition of acetic acid to reaction results in the formation of A (47%) along with B (41%) for 1b, which is

View Article Online
DOI: 10.1039/C9DT02518A

higher than 2b A(31%) along with B (34%)and 3b A(26%) along with B (28%). The addition of the radical scavenger TEMPO (2,2,6,6-tetramethylpiperidin-1-yl-oxyl) to the reaction of 1b with O_2 showed no perceptible change in the product yields under identical reaction condition, which eliminates the possibility of radical based reaction pathways.[27] In two identical dioxygenation reactions were performed for 1b and their headspaces were purged separately into a saturated solution of $Ca(OH)_2$ and $PdCl_2$ leads to formation $CaCO_3$ and Pd precipitate respectively, which confirms CO_2 and CO formation during the reaction.[7,23a] Evolution of $CO_{2(g)}$ from the reaction mixture attributes to the formation of benzoic acid from the oxidative decomposition of phenyl glyoxal due to excess dioxygen used (Scheme 4; Path 1). Time-dependent product analysis for 1b with dioxygen was performed over various time intervals (Table S5) and showed yields A, 17%, B, 11%; A, 29%, B, 19%; A, 36%, B, 25% over 3, 6 and 9 hours respectively. The yields of benzoic acid and benzoin are seemingly independent over these reaction time under similar conditions. This result suggests that a remote possibility for the conversion of benzoin into benzoic acid. Further, the reaction of equimolar benzoin and complex 1 in the presence of dioxygen showed almost no formation of benzoic acid, which rules out the possibility of benzoic acid formation via benzoin. The source of oxygen is verified by using $^{18}O_2$ instead of $^{16}O_2$ and exhibited a shift of two mass units for benzoic acid (GC-MS, *m/z*, 124) with 47% isotopic incorporation ($^{16}O/^{18}O$ = 53:47) (Figure 4).[28] Thus, only one of the atoms of the $^{18}O_2$ molecule has been incorporated into the product benzoic acid and another one presumably eliminated as labeled CO/CO_2 (Scheme 3). The low incorporation of ^{18}O may be due to hydrolysis of triketone intermediate or exchange of ^{18}O with formed carboxylic acid.[29] Similarly when the reaction performed using an excess of $H_2{}^{18}O$ and in presence of dioxygen has shown only 2.7% of labeled benzoic acid (Figure S78). This little incorporation of ^{18}O into formed (^{16}O) benzoic acid must be resultant from partial hydrolysis/exchange of ^{18}O over the longer reaction time.[29a] Benzoin formation (A) from dioxygenation reaction invariably attributes that triketone being one among transient intermediate, which on subsequent decay by Lewis acid promoting benzoyl migration with the evolution of CO (Scheme 4).[7,30a] Thus, these results are suggesting that C-C bond breaking presumably proceeds via the initial formation of Fe^{II}-organoperoxidate intermediate.[14] Earlier studies on the enzyme were also suggesting a very similar mechanism for C-C bond cleavage.[13-15] In contrast to this, Solomon and co-workers have reported a Fe-mediated O_2 activation mechanism by the involvement of higher oxidation (Fe^{IV}=O) intermediate formed via the Fe^{3+}-$O^{2-\cdot}$ species.[16] On the

View Article Online
DOI: 10.1039/C9DT02518A

other hand, the involvement of multiple spin states of the metal center and its crucial role in controlling the reactivity via magnetic exchange coupling with bound oxygen have been established computationally for biomimetic models of other dioxygenase enzymes.[31] However, the accurate prediction of key intermediate and nature of the spin state of iron center needs further experimental and computational investigations.

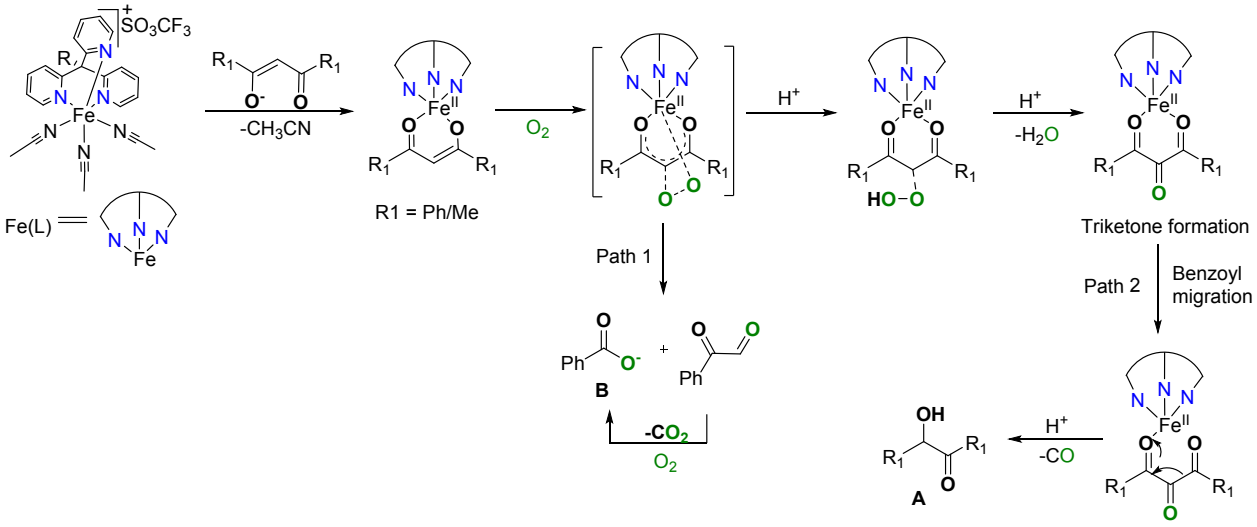

Scheme 4. The proposed reaction pathway.

Summary

In summary, the structurally well-defined models for the iron(II)-dependent DKDO enzyme have been synthesized and characterized. The molecular structure of the complexes and their electronic spectral signatures of substrate adducts showed a very similar coordination environment as similar to the active site and substrate adduct of native Fe(II)-DKDO enzyme. The $Fe^{2+/3+}$ redox potentials of complexes and their substrate adducts showed higher redox potentials than a reported redox barrier for dioxygen activation. The dioxygenation reaction has been accelerated 20 – 50 fold by the addition of H^+ (acetic acid). This is unambiguously exhibiting a relevant correlation with the rate of dioxygenation by native DKDO enzyme, where the glutamate residue (Glu98) facilitates the binding of substrate and its dioxygenation reactions from secondary coordination sphere as a pH regulating channel. Interestingly, the oxidation state of Fe(II) center is unaltered during the dioxygenation reaction as proposed similar to the native enzyme. Thus, kinetic studies and product analyses are revealing that the mechanism possibly proceeds via initial formation of Fe^{II}-organoperoxidate intermediate pathway as suggested for the DKDO enzyme.

View Article Online
DOI: 10.1039/C9DT02518A

The dioxygenation reaction of the phenyl substituted adducts yielded benzoin and benzoic acid as a major cleavage product with the evolution of CO and CO_2.

Experimental Section

Materials: The chemicals 2-ethylpyridine, 2-fluoropyridine, di-2-pyridylketone, *n*-butyl-lithium (2 M in hexane), iron(II) trifluromethane-sulfonate, iron(III) perchlorate hydrate, zinc(II) perchlorate hexahydrate, copper(II) trifluoromethane sulfonate, manganese(II) trifluromethane-sulfonate, acetic acid, acetylacetone, 1,3-diphenylpropane-1,3-dione, (diacetoxy-iodo)benzene $PhI(OAc)_2$, $H_2{}^{18}O$ and *tert*-butyl hydroperoxide (*t*-BuOOH) were purchased from Sigma-Aldrich. $^{18}O_2$ was purchased from Cambridge Isotope Laboratories. The supporting electrolyte tetrabutylammonium perchlorate (TBAP) was prepared in water and recrystallized twice from aqueous ethanol. Oxidant iodosobenzene (PhIO) was synthesized from $PhI(OAc)_2$. Anhydrous acetonitrile, 2-bromo pyridine, iodomethane, (Alfa Aesar), Tetrahydrofuran (THF) (Merck, India) were used as received. Dry THF obtained by literature method,[32] THF was refluxed for 1 hour over sodium metal and benzophenone and then distilled under N_2 atmosphere. The distilled solvent was degassed and stored under argon over molecular sieves.

Experimental conditions and physical measurements: All workups were carried out under dry argon using a standard Schlenk line or glove box techniques for the reactions involving air-sensitive synthesis and experiments. All NMR spectra were recorded on a Bruker 300 MHz spectrometer. Chemical shift values are given in parts per million (ppm). High-resolution electron impact mass spectra (HR-ESI MS) have been measured on a Bruker 12 Tesla APEX-Qe FTICR-MS (or) HRMS-ESI-Q-TOF LC/MS system. Elemental analyses were carried out using a Heraeus Vario Elemental automatic analyzer. UV-Vis spectra were recorded on an Agilent 8453 spectrometer with a cooling unit by Unisoku (Osaka, Japan). The Electrochemical data were recorded in Biologic SP-150 Electrochemical workstation. The potential was externally calibrated against the ferrocene/ferrocenium couple prior to analysis. The ESI-MS measurement was carried out on Thermo Fischer LC-MS. The ESI-MS & GC-MS measurement was carried out on Thermo Fischer LC-MS & Agilent 5977E GCMSD respectively. All pH measurements are made with the addition of 10% of aqueous acetonitrile solution. FT-IR was recorded on a Thermo Nicolet 6700 FT-IR spectrometer. The EPR experiments were made with a Biospin ELEXSYS E500

View Article Online
DOI: 10.1039/C9DT02518A

spectrometer (Bruker, Karlsruhe, Germany). The EPR spectrometer was equipped with a continuous-flow liquid He cryostat and an ITC503 temperature controller made by Oxford Instruments.

Evans Method Measurements: The effective magnetic moment was determined by using Evans'method.[33] In a typical experiment, an oxygen-free solution of a complex in d_6-DMSO, containing 5% tert-butanol by volume was placed in an NMR tube, while a reference solution of 5% tert-butanol (v/v) in d_6-DMSO, was placed into NMR tube insert. Then ^{1}HNMR experiments were performed on the Bruker 300 MHz spectrometer and magnetic moment values were obtained by fitting the chemical shift values in the standard equation of Evan's method.

Crystal Structure Determination of 1: All the measurements were performed using monochromatized Mo K_α radiation at 100K: $(C_{23}H_{24}FeN_6^{+2})_2(CF_3O_3S^-)_4 \cdot C_2H_3N$, M_r 1517.99, triclinic, space group P 1, a = 11.8586(6)Å, b = 12.4140(6)Å, c = 12.6961(6)Å, α = 60.817(2)°, β = 83.284(2)°, γ = 73.222(2)°, V = 1561.69(14)Å^3, Z = 1, d_{calc} = 1.614g cm^{-3}, μ = 0.704 mm^{-1}. A total of 13837 reflections were collected (Θ_{max} = 28.0°), from which 10107 were unique (R_{int} = 0.0227), with 9675 having I > 2σ(I). The structure was solved by direct methods (SHELXS-97) and refined by full-matrix least-squares techniques against F^2 (SHELXL-2014/6).[34,35] Since racemic twinning was detected the structure was refined as a 2-component inversion twin resulting in a scale factor of 0.301(20) between the two unequal components. The size of the voids occupied by the four anions and the solvent molecule was computed to approx. 114, 110, 111, 136, and 104 Å^3, respectively. The CF_3 group of the anion in the largest void (including S4) was disordered over two orientations and was refined with site-occupation factors of 0.597(6) and 0.403(6), respectively. The same anisotropic displacement parameters were refined for equivalent atoms in the disordered part, and the equivalent bonds were restrained to have the same lengths. The other non-hydrogen atoms were refined with anisotropic displacement parameters without any constraints. The H atoms of the pyridine rings were put at the external bisectors of the X–C–C angles at C–H distances of 0.95Å and common isotropic displacement parameters were refined for the H atoms of the same ring. The H atoms of the methyl groups were

View Article Online
DOI: 10.1039/C9DT02518A

refined with common isotropic displacement parameters for the H atoms of the same group and idealized geometries with tetrahedral angles, enabling rotation around the C–C bond, and C–H distances of 0.98Å. For 870 parameters final *R* indices of R1 = 0.0400 and wR^2 = 0.1129 (GOF = 1.045) were obtained. The largest peak in a difference Fourier map was 0.846e$Å^{-3}$. CCDC-1522488 contains the supplementary crystallographic data for this paper.

Synthesis of Ligands

Synthesis of tris(2-pyridyl)ethane (L1): The ligand tris(2-pyridyl)ethane (L1) was synthesized by the early report with slight modifications.[24a] The solution of *n*-BuLi (14 mL, 28.0 mmol of 2 M in hexane) was added dropwise via syringe over 15 minutes to 2-ethyl pyridine (1.6 mL, 12.0 mmol) which was pre-cooled to -78˚C in THF (40 mL) under argon atmosphere. Then it was stirred vigorously and the temperature maintained below -70˚C. After 1 hour, the solution turns into a deep red color and then 2-fluoro pyridine (0.5 mL, 6 mmol) was added dropwise at -20˚C. The temperature was slowly elevated into room temperature. Over 30 minutes and refluxed for an additional 30 minutes. Further, another equivalent of 2-fluoro pyridine was added at 0˚C and subsequently refluxed for 2 hours. Finally, the reaction was quenched with water at 0˚C and organics were extracted with ethylacetate. Volatiles were removed by *vacuum.* Pure off-white crystalline solids were obtained by column chromatography using silica (7:3 hexane: ethyl acetate) with a yield of 72% (1.13 g). ^{1}H NMR ($CDCl_3$, 300 MHz): δ(ppm) 2.33 (s, 3H, CH_3), 7.10 (m, 6H), 7.59 (m, 3H) 8.58 (d, 3H); ^{13}C NMR ($CDCl_3$, 75 MHz) δ(ppm) 27.26 (CH_3), 59.99 (C-CH_3), 121.21, 123.43, 135.99, 149.00, 165.72. ESI-Mass, *m/z,* 261.05.

Synthesis of tris(2-pyridyl)methanol (L2): The ligand (L2) tri(2-pyridyl)methanol was also synthesized by the early report with slight modifications.[24b] To a pre-cooled 2-bromopyridine (4.60 g, 28 mmol) in THF (175 mL) *n*-BuLi (20 mL, 28 mmol of 2.0 M in hexane) was added dropwise with vigorous stirring at a temperature below -70°C under argon atmosphere. This reaction mixture was stirred for 30 minutes and then di-2-pyridyl ketone (2.54 g, 13.8 mmol) in THF (25 mL) was added. The further stirring of solution for an additional hour shows a change of color deep red into violet. At this stage, the reaction was quenched by adding methanol-water mixture at 0˚C and organics were separated with ethyl acetate. The removal of ethyl acetate under *vacuum* yielded pure off-white crystalline solid, yield: 92% (3.30 g). ^{1}H NMR ($CDCl_3$, 300 MHz): δ (ppm) 7.19

View Article Online
DOI: 10.1039/C9DT02518A

(td, 3H), 7.71 (m, 6H) 8.58 (dd, 3H); ^{13}C NMR ($CDCl_3$, 75 MHz) δ (ppm) 81.21 (C-OH), 122.27, 122.90, 136.38, 147.77, 162.80. ESI-MS, *m/z*, 263.05.

Synthesis of tris(2-pyridylmethoxy)methane (L3): The ligand (L3) tris(pyridyl-2-methoxy)methane has been synthesized by adding NaH (0.83 g, 0.03 mol) to tris-pyridylcarbinol in DMF and followed by the dropwise addition of iodomethane (0.40 mL, 0.9 g, 0.0065 mol) at room temperature. The reaction mixture was stirred for 1.5 hours and quenched with a 1:1 mixture of acetone and 2-propanol. After addition of water, the organic solvents are removed under vacuum. The product was extracted with CH_2Cl_2 and recrystallized from acetone to give a crystalline white solid (yield, 48%, 1.5 g). ^{1}H NMR ($CDCl_3$, 300 MHz): δ (ppm) 7.19 (td, 3H), 7.71 (m, 6H) 8.58 (dd, 3H); ^{13}C NMR ($CDCl_3$, 75 MHz) δ(ppm) 81.21 (C-OH), 122.27, 122.90, 136.38, 147.77, 162.80.

Synthesis of iron(II) complexes: All the iron(II) complexes were synthesized under dry argon using standard Schlenk line and glove box. The ligand (0.5 mmol) was added to iron(II) trifluoromethanesulfonate (0.176 g, 0.5 mmol) in acetonitrile (10 mL). The reaction mixture was stirred for 2 hours and removal of solvent under *vacuum* yielded red-orange color solid. Then, it was washed with diethyl ether to remove the free ligand.

$[Fe(L1)(CH_3CN)_3](SO_3CF_3)_2$, 1: Yield, 0.30 g, 82%, HR-ESI Mass, *m/z,* 466.01309 corresponds to $[Fe(L1)(SO_3CF_3)]^+$ ion. $[Fe(L1)(CH_3CN)_3](SO_3CF_3)_2$, 1: Analytically calculated for $C_{25}H_{24}F_6FeN_6O_6S_2$: C, 40.66; H, 3.28; N, 11.38%. Found: C, 40.28; H, 3.62; N, 11.47%. ^{1}H NMR (CD_3CN, 300 MHz): δ (ppm) 18.66, 15.97, 14.1, 8.98, 4.3.

$[Fe(L2)(CH_3CN)_3](SO_3CF_3)_2$, 2: Yield, 0.27 g, 74%, HR-ESI Mass, *m/z,* 467.99263 corresponds to $[Fe(L2)(SO_3CF_3)]^+$ ion. $[Fe(L2)(CH_3CN)_3](SO_3CF_3)_2$ 2: Analytically calculated for $C_{24}H_{22}F_6FeN_6O_7S_2$: C, 38.93; H, 3.0; N, 7.54%. Found: C, 38.68; H, 3.20; N, 7.14%.^{1}HNMR (CD_3CN, 300 MHz): δ (ppm) 17.88, 15.57, 14.1, 8.88.

$[Fe(L3)(CH_3CN)_3](SO_3CF_3)_2$, 3: Yield, 0.28 g, 82%, HR-ESI Mass, *m/z,* 482.00789 corresponds to $[Fe(L3)(SO_3CF_3)]^+$ ion. $[Fe(L3)(CH_3CN)_3](SO_3CF_3)_2$ 3: Analytically calculated for $C_{25}H_{24}F_6FeN_6O_7S_2$: C, 39.80; H, 3.21; N, 11.14%. Found: C, 39.58; H, 3.17; N, 11.26%. ^{1}H NMR (CD_3CN, 300 MHz): δ (ppm) 19.06, 16.07, 14.3, 9.1, 3.67.

View Article Online
DOI: 10.1039/C9DT02518A

Synthesis of complex-acac adducts: The complex-acac adducts were synthesized by two steps as a previously reported method with suitable modifications.[20,21] The Na(acac^{X}) (X = Me, Ph) salts were prepared by the reaction of respective β-diketone (0.52 mmol) and NaH (0.52 mmol) in dry THF. Then, stirred for 30 minutes and the solvent was removed under vacuum to yield the Na(acac^{X}) salts as a white solid. In second step, $Fe(SO_3CF_3)_2$ (0.5 mmol) was added to ligand (0.5 mmol) in acetonitrile (10 mL) and then followed by addition of Na(acac^{X}) in acetonitrile. The reaction mixture was stirred overnight at room temperature. The solution was filtered to remove $NaSO_3CF_3$ and then evacuated to yield red-orange solids. The solids were washed with diethyl ether (3 × 3 mL) and dried under *vacuum* to yield pure adducts.

[Fe(L1)(acac^{Me})]SO_3CF_3, 1a: Yield, 0.13 g, 61%, ESI-MS, *m/z,* 416.11 corresponds to [Fe(L1)(acac^{Me})]$^+$ ion. 1a: Analytically calculated for $C_{23}H_{22}F_3FeN_3O_5S$: C, 48.86; H, 3.92; N, 7.43%. Found: C, 48.83; H, 3.90; N, 7.42%.; IR: $\bar{\upsilon}_{(CO)}$ - 1605 cm^{-1}.

[Fe(L1)(acac^{Ph})]SO_3CF_3, 1b: Yield, 0.16 g, 58%, HR-ESI mass, *m/z,* 541.9780 for corresponds to [Fe(L1)(acac^{Ph})]$^+$ ion. 1b: Analytically calculated for $C_{33}H_{26}F_3FeN_3O_5S$: C, 57.49%; H, 3.80%; N, 6.09%. Found: C, 57.51; H, 3.81; N, 6.07%; IR: $\bar{\upsilon}_{(CO)}$ - 1617 cm^{-1}.

[Fe(L2)(acac^{Me})]SO_3CF_3, 2a: Yield, 0.11 g, 53%, ESI-MS, *m/z,* 417.70 corresponds to [Fe(L2)(acac^{Me})]$^+$ ion. 2a: Analytically calculated for $C_{22}H_{20}F_3FeN_3O_6S$: C, 46.58; H, 3.55%; N, 7.41%. Found: C, 46.56; H, 3.54; N, 7.40%.; IR: $\bar{\upsilon}_{(CO)}$ – 1602 cm^{-1}.

[Fe(L2)(acac^{Ph})]SO_3CF_3, 2b: Yield, 0.13 g, 49%, HR-ESI mass, *m/z,* 541.6120 corresponds to [Fe^{II}(L2)(acac^{Ph})]$^+$ ion. 2b: Analytically calculated for $C_{32}H_{24}F_3FeN_3O_6S$: C, 55.58%; H, 3.50%; N, 6.08%. Found: C, 55.51; H, 3.48; N, 6.04%; IR: $\bar{\upsilon}_{(CO)}$ - 1619 cm^{-1}.

[Fe(L3)(acac^{Me})]SO_3CF_3, 3a: Yield, 0.1 g, 49%, HR-ESI mass, *m/z,* 432.0536 corresponds to [Fe(L3)(acac^{Me})]$^+$. 3a: Analytically calculated for $C_{23}H_{22}F_3FeN_3O_6S$: C, 47.52; H, 3.81; N, 7.23%. Found: C, 47.49; H, 3.79; N, 7.12%.; IR: $\bar{\upsilon}_{(CO)}$ - 1593 cm^{-1}

View Article Online
DOI: 10.1039/C9DT02518A

Kinetics studies and products analysis: The solutions of iron(II) complexes and substrate were prepared under an argon atmosphere in the Schlenk line. The kinetics of the dioxygenase reactions monitored by time-dependent measurements of the disappearance of the $Fe^{II} \rightarrow (acac^{X})$ MLCT bands at 25˚ C. The freshly prepared adducts were exposed to O_2 in acetonitrile solution. The solubility of O_2 in acetonitrile is 8.1×10^{-3} M.[28] The dioxygenase activities and product analysis of the present complexes was carried out in the separate experiments. The phenyl substituted adducts 1b - 3b (0.1 mmol) were exposed to O_2 in the presence of acetic acid and stirred for 12 hours. The oxygenation reaction was quenched by adding 6 M HCl (5 mL). Then the products were extracted using ethyl acetate (3×15 mL). The organic layer was dried over anhydrous Na_2SO_4 at room temperature. Further purification was performed using column chromatography using silica gel (8:2 hexane: ethyl acetate). The major products were separated and characterized by NMR and GC-MS analysis. Whereas, the reactions using *t*-BuOOH and $PhI(OAc)_2$ as oxidant were performed by an identical procedure over 3 hours only.

GC-MS: Benzoic acid: *m/z*, 150.13; ^{1}H NMR ($CDCl_3$, 300 MHz): δ (ppm) 8.14 (m, 2H), 7.63 (m, 1H) 7.48 (m, 2H); ^{13}C NMR ($CDCl_3$, 75 MHz) δ(ppm) 128.80, 130.61, 134.20, (C=O) 173.02. ^{1}H & ^{13}C NMR.

Benzil *m/z*, 210.05; ^{1}H NMR ($CDCl_3$, 300 MHz): δ (ppm) 8.1 (dd, 4H), 7.65 (m, 2H) 7.51 (m, 4H). Benzoin *m/z*, 212.05; ^{1}H NMR ($CDCl_3$, 300 MHz): δ (ppm) 8.14 (m, 4H), 7.63 (m, 6H) 5.6 (s, 1H). These data were good agreement with previously reported data in literature.

$^{18}O_2$ Labeling studies: In the separate experiments, 1b (0.1 mmol) was exposed to $^{18}O_2$ for 12 hours and stirred. The reaction was quenched with 0.1 mL of HCl and solvent was removed *in vacuo* under a nitrogen atmosphere. The products were extracted with ethyl acetate, passed through a short silica column and analyzed by GC-MS. GC-MS analysis performed on Agilent 5977E GCMSD using HP- 5 MS ultra-inert (30 m × 250 µm × 0.25 µm) capillary column.

Acknowledgment

We acknowledge Science and Engineering Research Broad (SERB), New Delhi and Board Research in Nuclear Sciences (BRNS), Mumbai for funding.

Conflict of interest

View Article Online
DOI: 10.1039/C9DT02518A

The authors have no conflict of interest

References

1 (a) S. Shoda, H. Uyama, J. Kadokawa, S. Kimura, S. Kobayashi, *Chem. Rev.* 2016, 116, 2307. (b) M. Sono, M. P. Roach, E. D. Coulter, J. H. Dawson, *Chem Rev* 1996, 96, 2841. (c) R. S Boethling, E. Sommer, D. DiFiore, *Chem. Rev.* 2007, 107, 2207.
2 (a) R. N. Armstrong, *Biochemistry* 2000, 39, 13625. (b) M. Costas, M. P. Mehn, M. P. Jensen, L. Que, *Chem. Rev.* 2004, 104, 939.(c) A. L. Feig, S. J. Lippard, *Chem. Rev.* 1994, 94, 759. (d) A. D. Liang, S. J. Lippard *J. Am. Chem. Soc.* 2015, 137, 10520.
3 (a) E. L. Hegg, A. K. Whiting, R. E. Saari, J. McCracken, R. P. Hausinger, L. Que, *Biochemistry* 1999,38, 16714. (b) A. Wójcik, M. Radoń, T. *J.* Borowski, *Phys. Chem. A* 2016, 120, 1261.
4 S. C. Chai, T. Ju, M. Dang, R. B.Goldsmith, M. J. Maroney, T. C. Pochapsky, *Biochemistry* 2008, 47, 2428.
5 A. R. Deshpande, K. Wagenpfeil, T. C. Pochapsky, G. A. Petsko, D. Ringe, *Biochemistry* 2016, 55, 1398.
6 M. J. Maroney, S. Ciurli, *Chem. Rev.* 2014, 114, 4206.
7 (a) C. J. Allpress, K. Grubel, E. Szajna-Fuller, A. M. Arif, L. M. Berreau, *J. Am. Chem. Soc.* 2013, 135, 659. (b) K. Rudzka, A. M. Arif, and L. M. Berreau *Inorg. Chem.*, 2008, 47, 10832.
8 E. I. Solomon, D. E. Heppner, E. M. Johnston, J. W. Ginsbach, J. Cirera, M. Qayyum, M. T. Kieber-Emmons, C. H. Kjaergaard, R. G. Hadt, L. Tian, *Chem. Rev.* 2014, 114, 3659.
9 G. D. Straganz, L. Brecker, H. J. Weber, W. Steiner, D. W. Ribbons, *Biochem. Biophys. Res. Commun.* 2002, 297, 232.
10 G. D. Straganz, A. Glieder, L. Brecker, D. W. Ribbons, W. Steiner, *Biochem. J.* 2003, 369, 573.
11 D. Buongiorno, G. D. Straganz, *Coord. Chem. Rev.* 2013, 257, 541.
12 H. Brkic, D. Buongiorno, M. Ramek, G. D. Straganz, S. Tomic, *J. Biol. Inorg. Chem.* 2012, 17, 801.
13 G. D. Straganz, B. Nidetzky, *ChemBioChem* 2006, 7, 1536.
14 G. D. Straganz, B. Nidetzky, *J. Am. Chem. Soc.* 2005, 127, 12306.
15 (a) A. R. Diebold, M. L. Neidig, G. R. Moran, G. D. Straganz, E. I. Solomon, *Biochemistry* 2010, 49, 6945. (b) G. D. Straganz, A. R. Diebold, S. Egger, B. Nidetzky, E. I. Solomon, *Biochemistry* 2010, 49, 996.
16 A. R. Diebold, G. D. Straganz, E. I. Solomon, *J. Am. Chem. Soc.* 2011, 133, 15979.
17 S. Leitgeb, B. Nidetzky, *ChemBioChem* 2010, 11, 502.
18 G. Grogan, *Biochem. J.* 2005, 388, 721.
19 N. Kitajima, N. Tamura, M. Ito, H.Amagai, Y. Moro-oka, K. Heerwegh, A. Penicaud, R. Mathur, C. A. Reed, P. D. W. Boyd, *Inorg. Chem.* 1993, 32, 3583.
20 S I. Siewert, C. Limberg, *Angew. Chem., Int. Ed.* 2008, 47, 7953.
21 (a) H. Park, J. S. Baus, S. V. Lindeman, A. T. Fiedler, *Inorg. Chem.* 2011, 50, 11978. (b) H. Park, M. Bittner, J. S. Baus, S. V. Lindeman, A. T. Fiedler, *Inorg. Chem.* 2012, 51, 10279
22 M. M. Bittner, J. S. Baus, S. V. Lindeman, A. T. Fiedler, *Eur. J. Inorg. Chem.* 2012, 1848.
23 (a) R. Ramasubramanian, K. Anandababu, M. Kumar, R. Mayilmurugan, *Dalton Trans.,* 2018, 47*,* 4049; (b) K. Anandababu, R. Ramasubramanian, H. Wadepohl, P. Comba, N. J. Britto, M. Jaccob, and Ramasamy Mayilmurugan, Chem. Eur. J. 2019, 25, 9540.

View Article Online
DOI: 10.1039/C9DT02518A

24 (a) E. A. Ünal, D. Wiedemann, J. Seiffert, J. P. Boyd, A. Grohmann, *Tetrahedron Lett.* 2012, 53, 54. (b) R. T. Jonas, T. D. P. Stack, *Inorg. Chem.* 1998, 37, 6615.
25 S. Leitgeb, G. D. Straganz, B. Nidetzky, *FEBS J.* 2009, 276, 5983.
26 (a) Y. M. Badiei, M. A.Siegler, D. P. Goldberg, *J. Am. Chem. Soc.* 2011, 133, 1274 and reference therein. (b) P. Comba, Y.-M Lee, W. Nam, A. Waleska, *Chem. Commun.* 2014, 50, 412.
27 Q. Xing, H. Lv, C. Xia, F. Li, *Chem. Commun.* 2016, 52, 489.
28 (a) D. T. Sawyer, Oxygen Chemistry; Oxford University Press: New York, 1991; (b) W. O. Koch, and H. J. Krüger, *Angew. Chem., Int. Ed.,* 1996, 34, 2671. (c) R. Mayilmurugan, H. Stoeckli-Evans, M. Palaniandavar, *Inorg. Chem.*, 2008, 47, 6645.
29 (a) M. L. Bender, R. R. Stone, and R. S. Dewey, *J. Am. Chem.Soc.*, 1956, 78, 319; (b) S. Paria, P. Halder and T. K. Paine, *Angew. Chem., Int. Ed.,* 2012, 51, 6195.
30 (a) J. D. Roberts, D. R. Smith, C. C. Lee, *J. Am. Chem. Soc.* 1951, 73, 618. (b) R. D. Jana, D. Sheet, S. Chatterjee, T. K. Paine *Inorg. Chem.* 2018, 57, 8769.
31 (a) S. Rana, J. P. Biswas, A. Sen, M. Clemancey, G. Blondin, J. M. Latour, G. Rajaraman, D. Maiti, *Chem. Sci.*, 2018, 9, 7843; (b) P. Comba, S. Wunderlich, *Chem. Eur. J.* 2010, 16, 7293; (c) A. Ansari, P. Jayapal, G. Rajaraman *Angew. Chem. Int. Ed.,* 2015, 54, 564.
32 B. S. Furniss, A. J. Hannaford, P.W. Smith, A. R. Tatchell, Vogel's Textbook of practical organic chemistry, 5th Edition. PEARSON Education Limited, New Delhi, 2004, p 40.
33 D. F. Evans *J. Chem. Soc.* 1959, 2003. b) Z. Xue, J. C. Daran, Y. Champouret, R. Poli, *Inorg. Chem.* 2011, 50*,* 11543.
34 C. K. Johnson, ORTEP. Report ORNL-3794. Oak Ridge National Laboratory, Tennessee, USA (1965)
35 (a) Sheldrick, G. M. A short history of SHELX. Acta Cryst. A64, 2008, 112; (b) Sheldrick, G. M. Crystal structure refinement with SHELXL. Acta Cryst. C71, 2015, 3.

View Article Online
DOI: 10.1039/C9DT02518A

Figures and Tables

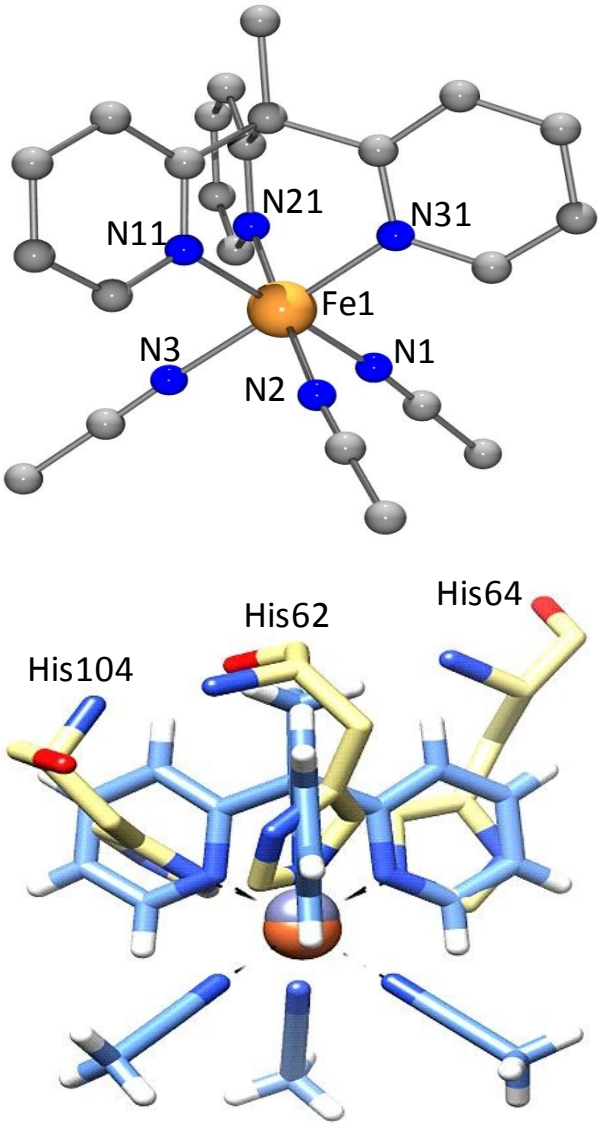

Figure 1. The molecular structure of 1 (50% probability factor of thermal ellipsoids). H atoms and $SO_3CF_3^-$ ions are omitted for clarity (top). Overlay plot of the structures of 1 and DKDO active site with Zn(II) cofactor (bottom).

View Article Online
DOI: 10.1039/C9DT02518A

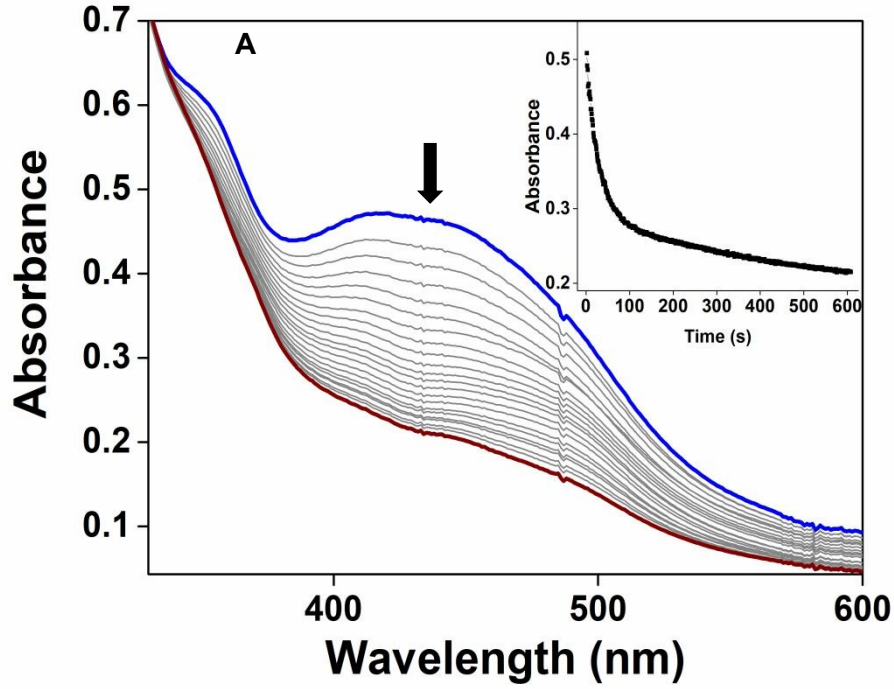

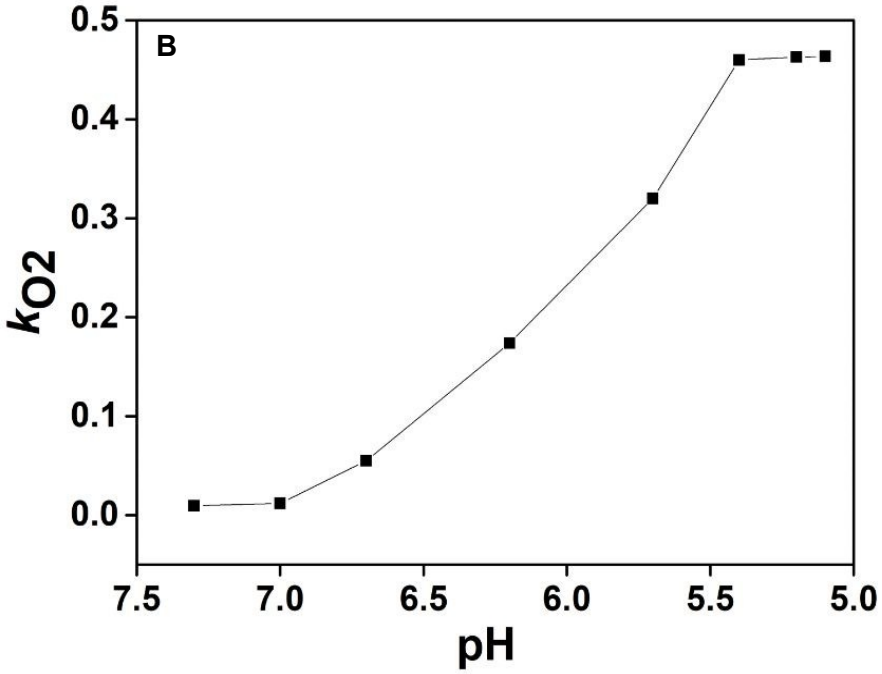

View Article Online
DOI: 10.1039/C9DT02518A

Figure 2. The progress of the reaction of 1a (6×10^{-4} M) with O_2 and 0.5 equiv. of acetic acid) in ammonium acetate in water/acetonitrile (3:7) buffer at 25°C. Inset: Plot of time vs absorbance (435 nm) (A). The plot of ko_2 vs pH (B) in ammonium acetate in water/acetonitrile (3:7) buffer.

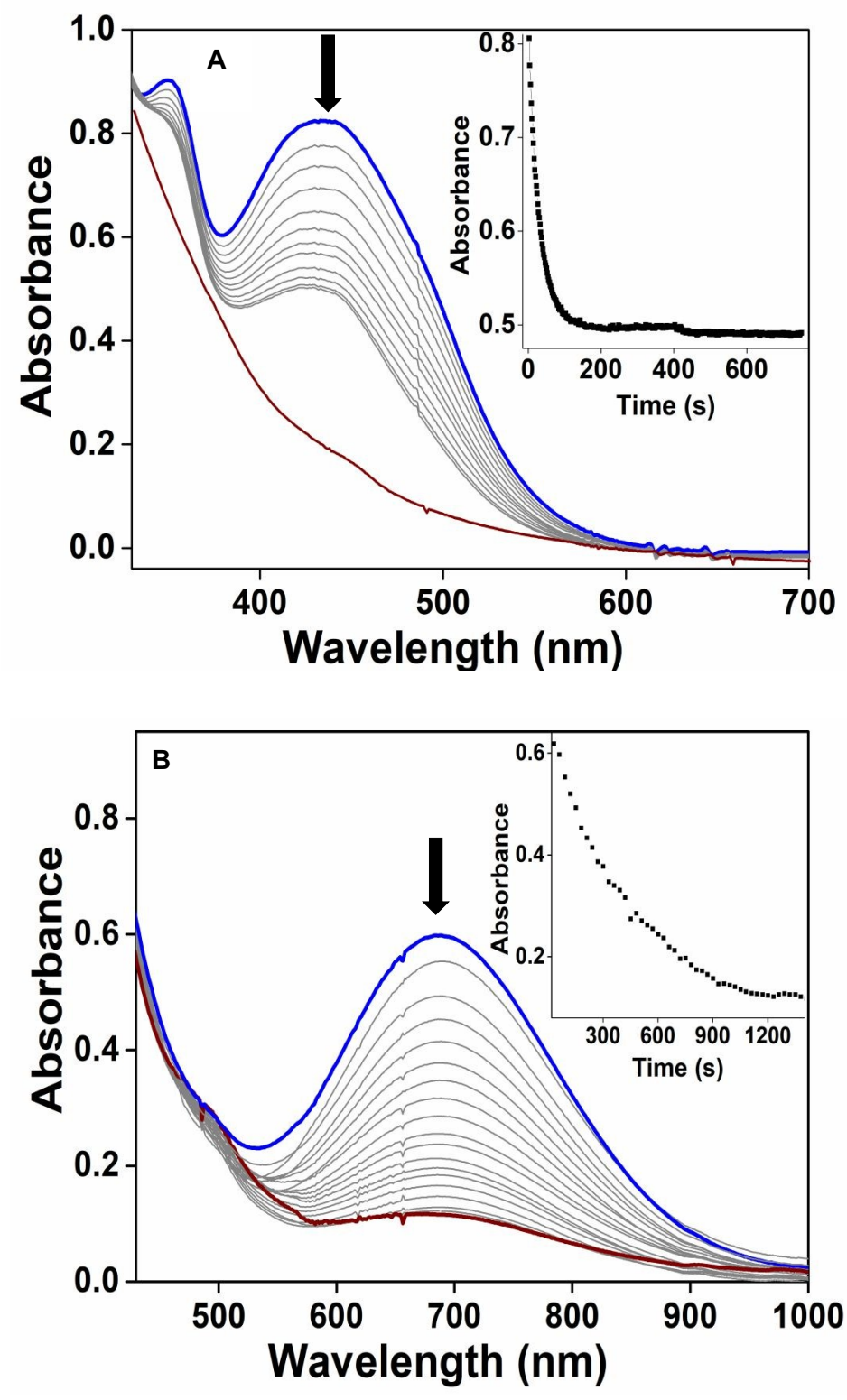

View Article Online
DOI: 10.1039/C9DT02518A

Figure 3. The progress of the reaction of 1a (6×10^{-4} M) with acetic acid (0.5 equiv) (A) in ammonium acetate in water/acetonitrile (3:7) buffer and 1 (6×10^{-4} M) (B) in the presence of *t*-BuOOH in acetonitrile at 25˚C. Insets: plots of time vs absorbance change.

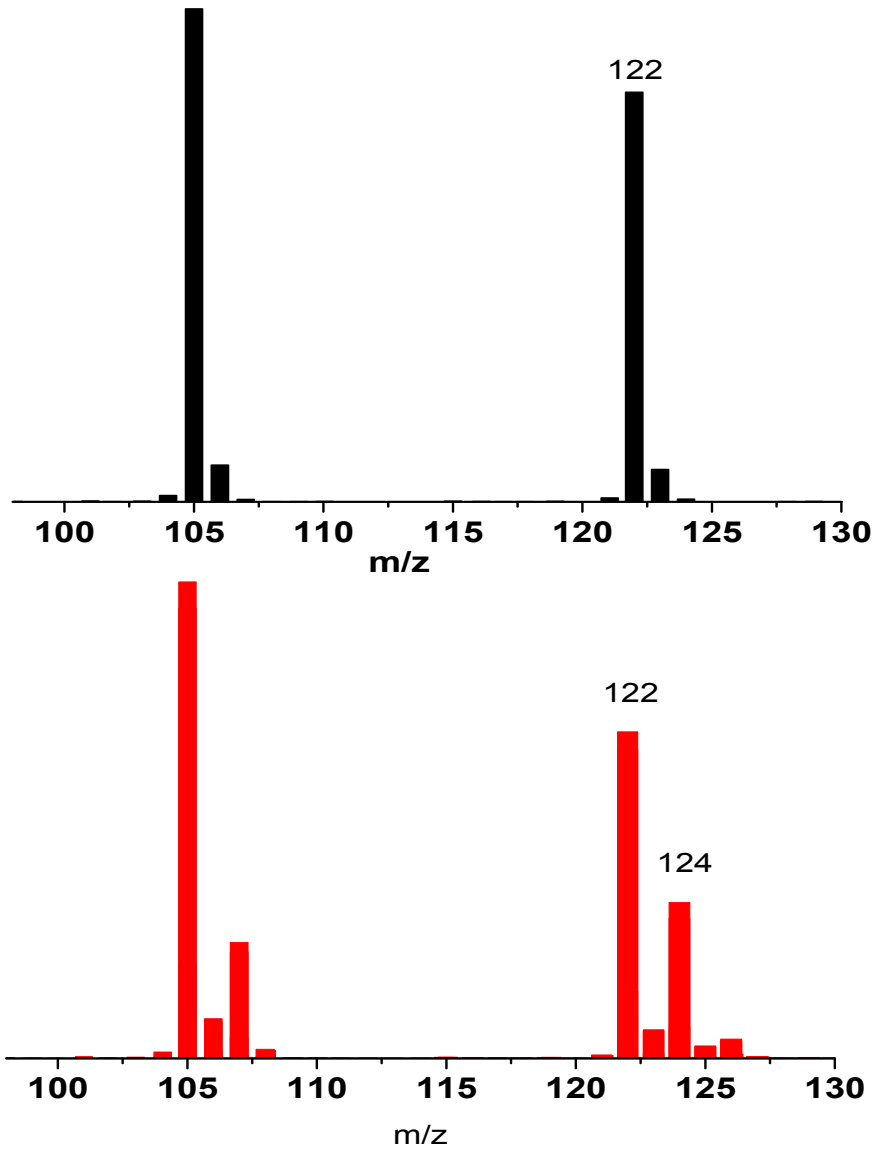

Figure 4. Oxygen isotopic studies for the reaction of 1b using $^{16}O_2$ (top) and with $^{18}O_2$ (bottom).

View Article Online
DOI: 10.1039/C9DT02518A

Table 1. Selected bond lengths [Å] and angles [°] for 1

1		1’	
Fe(1)-N(3)	1.948(4)	Fe(2)-N(51)	1.952(3)
Fe(1)-N(21)	1.952(4)	Fe(2)-N(43)	1.952(4)
Fe(1)-N(2)	1.954(3)	Fe(2)-N(41)	1.954(4)
Fe(1)-N(31)	1.958(4)	Fe(2)-N(71)	1.956(4)
Fe(1)-N(11)	1.959(3)	Fe(2)-N(61)	1.958(3)
Fe(1)-N(1)	1.961(4)	Fe(2)-N(42)	1.965(4)
N(11)-Fe(1)-N(1)	179.01(18)	N(51)-Fe(2)-N(41)	179.08(16)
N(21)-Fe(1)-N(2)	177.98(19)	N(61)-Fe(2)-N(42)	178.81(16)
N(31)-Fe(1)-N(3)	178.70(18)	N(71)-Fe(2)-N(43)	179.00(16)
N(3)-Fe(1)-N(21)	90.48(14)	N(51)-Fe(2)-N(43)	92.32(15)
N(3)-Fe(1)-N(2)	88.45(15)	N(43)-Fe(2)-N(41)	88.50(15)
N(21)-Fe(1)-N(31)	88.25(15)	N(51)-Fe(2)-N(71)	88.68(15)
N(2)-Fe(1)-N(31)	92.83(15)	N(41)-Fe(2)-N(71)	90.51(16)
N(3)-Fe(1)-N(11)	92.09(15)	N(51)-Fe(2)-N(61)	88.38(14)
N(21)-Fe(1)-N(11)	88.66(14)	N(43)-Fe(2)-N(61)	91.46(15)
N(2)-Fe(1)-N(11)	89.69(14)	N(41)-Fe(2)-N(61)	91.16(15)
N(31)-Fe(1)-N(11)	88.15(14)	N(71)-Fe(2)-N(61)	88.70(15)
N(3)-Fe(1)-N(1)	88.49(15)	N(51)-Fe(2)-N(42)	90.43(14)
N(21)-Fe(1)-N(1)	92.12(14)	N(43)-Fe(2)-N(42)	88.53(15)

Standard deviation in parenthesis.

View Article Online
DOI: 10.1039/C9DT02518A

Table 2. Electronic spectra[a] and redox data[b] for iron(II) complexes and their adducts in acetonitrile solution.

Complex	λ_{max}, nm (ε,M^{-1} cm^{-1})	υ_{st}[c] (cm^{-1})	Ep_a (V)	Ep_c (V)	ΔE (mV)	$E_{1/2}$ (V) CV	$E_{1/2}$ (V) DPV
1	470 (724) 378 (1870) 341 (183 $\times 10^2$) 259 (109 $\times 10^5$)	-	1.13	0.98	150	1.05	1.06
2	478 (219) 345 (1250) 341 (189$\times 10^2$) 259 (1112$\times 10^5$)	-	1.3	1.1	200	1.2	1.32
3	418 (402) 386 (1744) 340 (183$\times 10^2$) 263 (109$\times 10^5$)	-	1.24	1.05	190	1.14	1.2
1a	430 (305) 348 (507) 280 (146$\times 10^5$)	1605	1.12	0.97	-	1.04	1.05
1b	490 (628) 417 (1837) 341 (155$\times 10^2$) 249 (97$\times 10^5$)	1617	1.08	0.96	-	1.02	1.03
2a	440 (305) 338 (507) 278 (146$\times 10^5$) 221 (119$\times 10^5$)	1602	1.3	1.1	-	1.2	1.25
2b	485 (618) 413 (1878) 339 (135$\times 10^2$) 251 (102$\times 10^5$)	1619	1.27	1.12	-	1.12	-
3a	430 (305) 348 (507) 280 (146$\times 10^5$)	1593	1.25	1.08	-	1.17	1.2

View Article Online
DOI: 10.1039/C9DT02518A

[a]Concentration of iron(II) complexes, 1 × 10^{-3} M; Ligand-based transitions were measured in 1 × 10^{-7} M.[b]Electrochemistry: concentration of complexes:1 ×10^{-3} M; TBAP (0. 1 M) as supporting electrolyte in acetonitrile. Ag(s)/Ag^{+} (0.01 M, 0.10 M TBAP) as reference electrode; add 0.681 V to convert to NHE. Platinum disc and platinum wire were used as working and counter electrodes respectively. Scan rate: 100 mV s^{-1} calibrated with ferrocene. [c]carbonyl stretching frequency

Table 3. Kinetic data and isolated yields for oxidative cleavage of complex-substrate adducts in CH_3CN

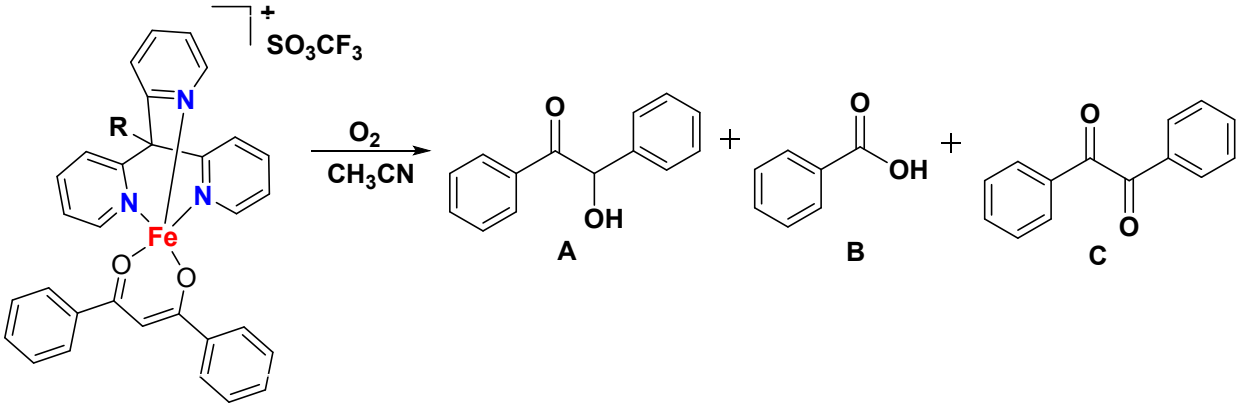

1b, R= -Me
2b, R = -OH
3b, R= -OMe

Adduct + O_2		pH	k_{obs} (× 10^{-5} s^{-1})	k_{O2} (× 10^{-3} M^{-1} s^{-1})	$t_{1/2}$ (h)[a]	Cleavage products (%)[b]
1a	-	7.4	7.34 ±0.02	9.41 ± 0.09	2.62	ND
	H^+	5.4	360.18 ±0.47	460 ± 0.66	0.05	ND
2a	-	7.3	3.83 ± 0.014	4.92 ± 0.07	5.02	ND
	H^+	5.3	133.33 ±0.36	170.28±0.50	0.14	ND
3a	-	7.4	4.20 ± 0.01	5.37 ± 0.09	4.58	ND
3a	H^+	5.4	86.32 ± 0.29	110.24± 0.21	0.22	ND
1b	H^+	5.1	0.26 ± 0.01	0.332 ± 0.08	74.03	A(42), B (29)
2b	H^+	5.0	0.062 ± 0.03	0.079 ± 0.23	310.4	A(26), B (24)
3b	H^+	5.1	0.057 ± 0.02	0.0772± 0.15	337.7	A(18),B (22)

[a]k_{O2} = k_{obs}/[O_2]. [O_2] in CH_3CN, 8.1×10^{-3} M; $t_{1/2}$= 0.693/ k_{obs}; [b]Isolated yields. ND – not detected. H^+: the half equivalent of acetic acid

View Article Online
DOI: 10.1039/C9DT02518A

Bioinspired Models for an Unusual 3-Histidine Motif of Diketone Dioxygenase Enzymes

Ramamoorthy Ramasubramanian,[a] Karunanithi Anandababu,[a] Nadia C. Mösch-Zanetti,[b] Ferdinand Belaj[b] and Ramasamy Mayilmurugan[a]*

Iron(II) complexes of tris-pyridine ligands have been showed as accurate models for an unusual 3-His motif of DKDO. Their diketonate adducts were showed regioselective C-C cleavage with O_2.